Spontaneous magnon decay in two-dimensional altermagnets

Niklas Cichutek, Peter Kopietz, and Andreas Rückriegel*
Institut für Theoretische Physik, Universität Frankfurt, Max-von-Laue Straße 1, 60438 Frankfurt, Germany

(Received 7 March 2025; accepted 14 July 2025; published 2 September 2025)

We show that magnons in two-dimensional altermagnets can spontaneously decay at zero temperature. The decay rate is determined by quantum fluctuations and scattering processes involving the decay of a single magnon into three. These processes are kinematically allowed due to the convexity of the altermagnetic magnon dispersion. For small wave vectors k, the decay rate is proportional to k^5 with a direction-dependent prefactor, which is maximal along the diagonals of the Brillouin zone. Moreover, for a given momentum only magnons with one specific chirality can spontaneously decay.

DOI: 10.1103/b5vs-ldpm

I. INTRODUCTION

The spontaneous decay of quasiparticles at zero temperature is a fundamental manifestation of quantum mechanics in condensed matter. In general, this is only possible if the ground state exhibits zero-point (quantum) fluctuations and the quasiparticle dispersion $\omega_{\boldsymbol{k}}$ is a convex function of the momentum $\boldsymbol{k}$ so that the decay of a single quasiparticle into two or more quasiparticles is kinematically allowed. A well-known example where both conditions are satisfied is the quasiparticle decay in the superfluid ground state of interacting bosons [1]. In this case, the low-energy quasiparticles are phonons with long-wavelength dispersion $\omega_{\boldsymbol{k}} = ck + \alpha k^3$, where the sound velocity c and the coefficient α of the cubic nonlinearity are positive, implying that $\omega_{\boldsymbol{k}}$ is a convex function of $k = |\boldsymbol{k}|$. The dominant scattering process, which determines the so-called Beliaev damping [2] of the phonons at zero temperature, involves the decay of one phonon into two. In three dimensions, the corresponding decay rate is proportional to k^5 at long wavelengths [1], which generalizes to k^{2d-1} in $d > 1$ dimensions [3].

In the above example, the convexity of the quasiparticle dispersion guarantees that the relevant decay process satisfies energy and momentum conservation. Conversely, quasiparticles with a concave dispersion cannot spontaneously decay at zero temperature, even if the ground state exhibits quantum fluctuations. This is the reason why magnons in quantum Heisenberg antiferromagnets with nearest-neighbor exchange on a square lattice are stable at zero temperature [4,5]. In this work, we show that in some sectors of the Brillouin zone, such a kinematic constraint does not apply to magnons in the recently discovered altermagnets [6–8], so that magnons in altermagnets can, in fact, spontaneously decay. For simplicity, we focus here on two-dimensional altermagnets and show that the corresponding decay rate is dominated by the decay of one magnon into three. For small momenta, the decay rate is proportional to k^5 and depends on the direction in momentum space [9]. Interestingly, magnon decay in altermagnets is found to be *chirality selective* in the sense that for fixed $\boldsymbol{k}$ only the magnons with one specific chirality can spontaneously decay, while the magnons with the opposite chirality are stable. Spontaneous magnon decay in altermagnets has recently been discussed in Ref. [10]; however, an analytic understanding of the underlying physical mechanism has not been obtained.

II. MINIMAL SPIN MODEL

Starting point of our investigation is a minimal spin model for two-dimensional altermagnets on a square lattice with Hamiltonian [11]

$$\begin{aligned}\mathcal{H} = J \sum_{\boldsymbol{R}} \boldsymbol{S}_{\boldsymbol{R}} \cdot \left(\boldsymbol{S}_{\boldsymbol{R}+\boldsymbol{a}_1} + \boldsymbol{S}_{\boldsymbol{R}+\boldsymbol{a}_2}\right) \\ + \sum_{\boldsymbol{R}\in A} \boldsymbol{S}_{\boldsymbol{R}} \cdot \left(D\boldsymbol{S}_{\boldsymbol{R}+\boldsymbol{d}_1} + E\boldsymbol{S}_{\boldsymbol{R}+\boldsymbol{d}_2}\right) \\ + \sum_{\boldsymbol{R}\in B} \boldsymbol{S}_{\boldsymbol{R}} \cdot \left(E\boldsymbol{S}_{\boldsymbol{R}+\boldsymbol{d}_1} + D\boldsymbol{S}_{\boldsymbol{R}+\boldsymbol{d}_2}\right). \end{aligned} \tag{1}$$

where $\boldsymbol{S}_{\boldsymbol{R}}$ are spin-S operators localized at sites $\boldsymbol{R}$ of a square lattice with N sites, lattice spacing a, and basis vectors $\boldsymbol{a}_1 = a\hat{\boldsymbol{x}}$ and $\boldsymbol{a}_2 = a\hat{\boldsymbol{y}}$. We have divided the lattice into two sublattices A and B as shown in Fig. 1. The antiferromagnetic exchange coupling $J > 0$ connects all pairs of nearest-neighbor spins, while the diagonal coupling D connects spins across the diagonals $\boldsymbol{d}_1 = a(\hat{\boldsymbol{x}} + \hat{\boldsymbol{y}})$ and $\boldsymbol{d}_2 = a(-\hat{\boldsymbol{x}} + \hat{\boldsymbol{y}})$ on half of the plaquettes. On the diagonals of the other plaquettes, the spins are connected by a different coupling E such that the distinct plaquettes form a checkerboard pattern as illustrated in Fig. 1. Physically, D and E describe next-nearest-neighbor exchange mediated by two different types of nonmagnetic atoms located at the centers of the corresponding plaquettes. By setting $E = 0$, we obtain the model proposed in Ref. [12].

Assuming that the next-nearest-neighbor couplings D and E are small compared with J, the spin configuration in the classical ground state is the usual Neél state where spins on

*Contact author: rueckriegel@itp.uni-frankfurt.de

Published by the American Physical Society under the terms of the Creative Commons Attribution 4.0 International license. Further distribution of this work must maintain attribution to the author(s) and the published article's title, journal citation, and DOI.

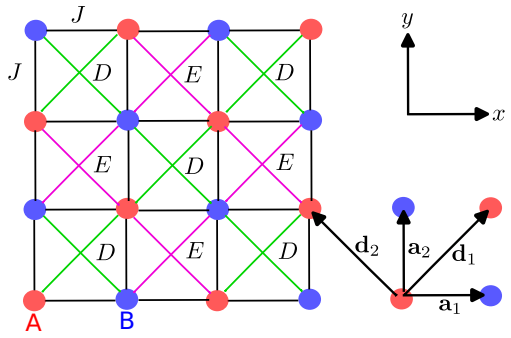


FIG. 1. Illustration of the spin model for an altermagnet on a square lattice defined in Eq. (1). The lattice is divided into two sublattices A and B. The exchange interaction J connects all pairs of nearest-neighbor spins, while the two types of couplings D and E connect the spins across the diagonals of plaquettes in a checkerboard pattern.

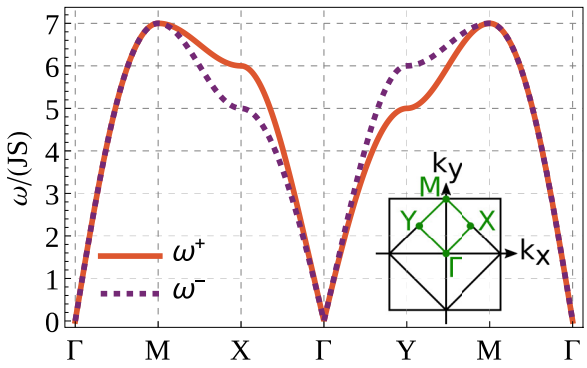


FIG. 2. Magnon dispersions $\omega_{\boldsymbol{k}}^{\pm}$ defined in Eq. (3) for the path in the Brillouin zone shown in the inset, where the M-point represents the wave vector $(0, \pi/a)$. The graph is for $D/J = -1/2$ and $E/J = -1/4$.

the two sublattices are collinear and point in opposite directions. The magnon spectrum can then be obtained by means of the usual steps: After bosonizing the spin operators via the Holstein-Primakoff transformation [13], we transform to momentum space and then use a Bogoliubov transformation to completely diagonalize the Hamiltonian. The quadratic part of the resulting magnon Hamiltonian is

$$\mathcal{H}_2 = \sum_{\boldsymbol{k}} (\omega_{\boldsymbol{k}}^{+} \alpha_{\boldsymbol{k}}^{\dagger} \alpha_{\boldsymbol{k}} + \omega_{\boldsymbol{k}}^{-} \beta_{\boldsymbol{k}}^{\dagger} \beta_{\boldsymbol{k}}), \tag{2}$$

where the sum is over the reduced Brillouin zone associated with the A-sublattice containing $N/2$ sites, $\alpha_{\boldsymbol{k}}$ and $\beta_{\boldsymbol{k}}$ are canonical annihilation operators for magnons with chirality $p = \pm$ and dispersions

$$\omega_{\boldsymbol{k}}^{p} = 4JS\epsilon_{\boldsymbol{k}} + p(E - D)2S \sin(k_x a) \sin(k_y a), \tag{3}$$

with

$$\epsilon_{\boldsymbol{k}} = \sqrt{(1 - \eta_{\boldsymbol{k}})^2 - \gamma_{\boldsymbol{k}}^2}, \tag{4a}$$

$$\eta_{\boldsymbol{k}} = \frac{D + E}{2J} [1 - \cos(k_x a) \cos(k_y a)], \tag{4b}$$

$$\gamma_{\boldsymbol{k}} = \frac{1}{2} [\cos(k_x a) + \cos(k_y a)]. \tag{4c}$$

A graph of the magnon dispersions is shown in Fig. 2. If k is small compared with the inverse lattice spacing, the magnon dispersions can be approximated by

$$\omega_{\boldsymbol{k}}^{\pm} = c|\boldsymbol{k}| \pm \frac{k_x k_y}{m} + \mathcal{O}(k^3), \tag{5}$$

with magnon velocity c and inverse mass $1/m$ given by

$$c = 2\sqrt{2} JSa \sqrt{1 - \frac{D + E}{J}}, \quad \frac{1}{m} = 2(E - D)Sa^2. \tag{6}$$

III. SPONTANEOUS MAGNON DECAY

For the calculation of the decay rate of the magnons, we have to express the quartic part $\mathcal{H}_4$ of the bosonized spin Hamiltonian in terms of magnon operators $\alpha_{\boldsymbol{k}}$ and $\beta_{\boldsymbol{k}}$, and the corresponding creation operators. A graphical representation of the resulting two-body Hamiltonian is shown in Fig. 3(a). The various scattering processes can be parametrized in terms of ten distinct interaction vertices $\Gamma^{(1A)}, \Gamma^{(1B)}, \ldots, \Gamma^{(5A)}, \Gamma^{(5B)}$ represented by the shaded squares. To exhibit the symmetries of the vertices, we normal-order $\mathcal{H}_4$ with respect to the α operators and antinormal order with respect to the β operators [14]. It is also convenient to introduce proper combinatorial factors to take into account the symmetries of the vertices with respect to permutations of external legs of the same type. It turns out that the spontaneous magnon decay rates are determined by scattering processes where one magnon decays into three ($1 \to 3$ process) or three magnons merge into one ($3 \to 1$ process). These processes are determined by the vertices $\Gamma^{(2A)}, \Gamma^{(2B)}, \Gamma^{(3A)}$, and $\Gamma^{(3B)}$ in the second line of Fig. 3(a) involving either one creation and three annihilation operators, or one annihilation and three

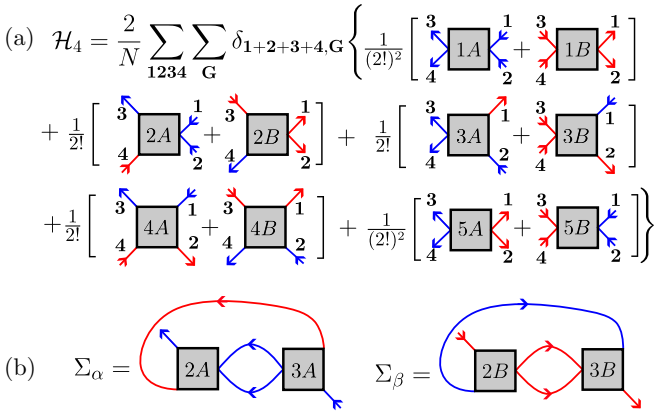


FIG. 3. (a) Graphical representation of the bosonized two-body Hamiltonian $\mathcal{H}_4$ of an altermagnet in terms of magnon operators. Here, bold numbers $\mathbf{1}, \mathbf{2}, \mathbf{3}$, and $\mathbf{4}$ represent the lattice momenta $\boldsymbol{k}_1$, $\boldsymbol{k}_2$, $\boldsymbol{k}_3$, and $\boldsymbol{k}_4$, respectively, which are conserved up to a vector $\boldsymbol{G}$ of the reciprocal lattice associated with the A-sublattice, i.e., $e^{i\boldsymbol{G}\cdot\boldsymbol{R}} = 1$ for $\boldsymbol{R} \in A$. Outgoing/incoming blue arrows represent $\alpha_{-\boldsymbol{k}}^{\dagger}/\alpha_{\boldsymbol{k}}$, while outgoing/incoming red arrows represent $\beta_{-\boldsymbol{k}}^{\dagger}/\beta_{\boldsymbol{k}}$. Arrows entering or leaving a vertex at the same point indicate that the vertex is symmetric with respect to the exchange of the corresponding momenta. (b) Diagrammatic representation of the two-loop corrections to the magnon self-energies at zero temperature. Internal lines with arrows represent imaginary-frequency magnon propagators.

creation operators. For the calculation of the spontaneous decay rate of the α magnons, we only need the vertex $\Gamma^{(2A)}$, which for general Umklapp momentum $\boldsymbol{G}$ is explicitly given by

$$\begin{aligned}\Gamma^{(2A)}_{\boldsymbol{G}}(\mathbf{3};\mathbf{4};\mathbf{2},\mathbf{1}) = 2J[&(u_{\mathbf{3}}u_{\mathbf{4}}\gamma_{\mathbf{2}+\mathbf{4}} + v_{\mathbf{3}}v_{\mathbf{4}}\gamma_{\mathbf{2}+\mathbf{3}})v_{\mathbf{2}}u_{\mathbf{1}} + (u_{\mathbf{3}}u_{\mathbf{4}}\gamma_{\mathbf{1}+\mathbf{4}} + v_{\mathbf{3}}v_{\mathbf{4}}\gamma_{\mathbf{1}+\mathbf{3}})u_{\mathbf{2}}v_{\mathbf{1}}\\ &+ s_{\boldsymbol{G}}(v_{\mathbf{3}}v_{\mathbf{4}}\gamma_{\mathbf{2}+\mathbf{4}} + u_{\mathbf{3}}u_{\mathbf{4}}\gamma_{\mathbf{2}+\mathbf{3}})u_{\mathbf{2}}v_{\mathbf{1}} + s_{\boldsymbol{G}}(v_{\mathbf{3}}v_{\mathbf{4}}\gamma_{\mathbf{1}+\mathbf{4}} + u_{\mathbf{3}}u_{\mathbf{4}}\gamma_{\mathbf{1}+\mathbf{3}})v_{\mathbf{2}}u_{\mathbf{1}}\\ &- u_{\mathbf{3}}v_{\mathbf{4}}(u_{\mathbf{2}}v_{\mathbf{1}}\gamma_{\mathbf{1}} + v_{\mathbf{2}}u_{\mathbf{1}}\gamma_{\mathbf{2}}) - (v_{\mathbf{3}}v_{\mathbf{4}}\gamma_{\mathbf{3}} + u_{\mathbf{3}}u_{\mathbf{4}}\gamma_{\mathbf{4}})u_{\mathbf{2}}u_{\mathbf{1}} - s_{\boldsymbol{G}}v_{\mathbf{3}}u_{\mathbf{4}}(v_{\mathbf{2}}u_{\mathbf{1}}\gamma_{\mathbf{1}} + u_{\mathbf{2}}v_{\mathbf{1}}\gamma_{\mathbf{2}})\\ &- s_{\boldsymbol{G}}(u_{\mathbf{3}}u_{\mathbf{4}}\gamma_{\mathbf{3}} + v_{\mathbf{3}}v_{\mathbf{4}}\gamma_{\mathbf{4}})v_{\mathbf{2}}v_{\mathbf{1}}] - u_{\mathbf{3}}v_{\mathbf{4}}u_{\mathbf{2}}u_{\mathbf{1}}W^{A}_{\mathbf{34};\mathbf{21}} - s_{\boldsymbol{G}}v_{\mathbf{3}}u_{\mathbf{4}}v_{\mathbf{2}}v_{\mathbf{1}}W^{B}_{\mathbf{34};\mathbf{21}}.\end{aligned} \tag{7}$$

Here, the usual Bogoliubov coefficients are given by

$$u_{\boldsymbol{k}} = \sqrt{\frac{1-\eta_{\boldsymbol{k}}+\epsilon_{\boldsymbol{k}}}{2\epsilon_{\boldsymbol{k}}}}, \quad v_{\boldsymbol{k}} = s_{\boldsymbol{k}}\sqrt{\frac{1-\eta_{\boldsymbol{k}}-\epsilon_{\boldsymbol{k}}}{2\epsilon_{\boldsymbol{k}}}}, \tag{8}$$

with $s_{\boldsymbol{k}} = \mathrm{sign}\gamma_{\boldsymbol{k}}$. The last two terms in Eq. (7) depend on the altermagnetic couplings D and E as follows:

$$\begin{aligned}W^{X}_{\mathbf{34};\mathbf{21}} = V^{X}_{\mathbf{1}+\mathbf{3}} + V^{X}_{\mathbf{1}+\mathbf{4}} + V^{X}_{\mathbf{2}+\mathbf{3}} + V^{X}_{\mathbf{2}+\mathbf{4}}\\ - V^{X}_{\mathbf{1}} - V^{X}_{\mathbf{2}} - V^{X}_{\mathbf{3}} - V^{X}_{\mathbf{4}}, \quad X = A, B,\end{aligned} \tag{9}$$

where $V^{A}_{\boldsymbol{k}} = D\cos(\boldsymbol{k}\cdot\boldsymbol{d}_1) + E\cos(\boldsymbol{k}\cdot\boldsymbol{d}_2)$ and $V^{B}_{\boldsymbol{k}} = E\cos(\boldsymbol{k}\cdot\boldsymbol{d}_1) + D\cos(\boldsymbol{k}\cdot\boldsymbol{d}_2)$. Note that the Hermiticity of the Hamiltonian implies that the vertex $\Gamma^{(3A)}$ can be obtained from $\Gamma^{(2A)}$ via complex conjugation,

$$\Gamma^{(3A)}_{\boldsymbol{G}}(\mathbf{3},\mathbf{4};\mathbf{2};\mathbf{1}) = \left[\Gamma^{(2A)}_{\boldsymbol{G}}(-\mathbf{2};-\mathbf{1};-\mathbf{3},-\mathbf{4})\right]^{*}. \tag{10}$$

Given the magnon Hamiltonian $\mathcal{H}_2 + \mathcal{H}_4$, we may now calculate the magnon self-energies using the imaginary time formulation of diagrammatic perturbation theory. To obtain the leading contribution to the magnon damping, we have to calculate all diagrams up to second order in the interaction $\mathcal{H}_4$. Let us focus on the diagonal self-energy $\Sigma_\alpha(\boldsymbol{k}, i\omega)$ of the α magnon with chirality $p = +$, where $i\omega$ is a bosonic Matsubara frequency. Due to the rather complicated interaction $\mathcal{H}_4$, eight distinct second-order diagrams contribute to $\Sigma_\alpha(\boldsymbol{k}, i\omega)$, which depend on various combinations of the interaction vertices. Fortunately, in the limit of vanishing temperature $T \to 0$, only the first diagram shown in Fig. 3(b) survives. This diagram has the unique property that the arrows attached to all external and internal lines point in the same direction. After evaluating the relevant frequency sums at finite T, we find that the contribution of this diagram to the self-energy of the α magnon can be written as

$$\begin{aligned}\Sigma_\alpha(\boldsymbol{k}, i\omega) = \frac{1}{2}\left(\frac{2}{N}\right)^2 \sum_{\boldsymbol{p},\boldsymbol{q}} [1 - e^{-(\omega^{+}_{\boldsymbol{p}}+\omega^{+}_{\boldsymbol{q}}+\omega^{-}_{\boldsymbol{k}-\boldsymbol{p}-\boldsymbol{q}})/T}]\\ \times W(\boldsymbol{p},\boldsymbol{q};\boldsymbol{k})\frac{(1+n^{+}_{\boldsymbol{p}})(1+n^{+}_{\boldsymbol{q}})(1+n^{-}_{\boldsymbol{k}-\boldsymbol{p}-\boldsymbol{q}})}{i\omega - \omega^{+}_{\boldsymbol{p}} - \omega^{+}_{\boldsymbol{q}} - \omega^{-}_{\boldsymbol{k}-\boldsymbol{p}-\boldsymbol{q}}},\end{aligned} \tag{11}$$

where $n^{\pm}_{\boldsymbol{p}} = 1/[e^{\omega^{\pm}_{\boldsymbol{p}}/T} - 1]$. The symmetry [Eq. (10)] implies that the relevant product of vertices is positive,

$$\begin{aligned}W(\boldsymbol{p},\boldsymbol{q};\boldsymbol{k}) &= \Gamma^{(2A)}_{0}(-\boldsymbol{k};\boldsymbol{k}-\boldsymbol{p}-\boldsymbol{q};\boldsymbol{p},\boldsymbol{q})\\ &\quad\times \Gamma^{(3A)}_{0}(-\boldsymbol{p},-\boldsymbol{q};\boldsymbol{k};\boldsymbol{p}+\boldsymbol{q}-\boldsymbol{k})\\ &= \left|\Gamma^{(2A)}_{0}(-\boldsymbol{k};\boldsymbol{k}-\boldsymbol{p}-\boldsymbol{q};\boldsymbol{p},\boldsymbol{q})\right|^2,\end{aligned} \tag{12}$$

where we have assumed that the external momentum $\boldsymbol{k}$ is sufficiently small so that we may set $\boldsymbol{G} = 0$ in all vertices. For $T \to 0$, Eq. (11) yields for the damping of the α magnons on resonance

$$\begin{aligned}\gamma_\alpha(\boldsymbol{k}) &= -\mathrm{Im}\,\Sigma_\alpha(\boldsymbol{k}, \omega^{+}_{\boldsymbol{k}} + i0^{+})\\ &= \frac{\pi}{2}\left(\frac{2}{N}\right)^2 \sum_{\boldsymbol{p},\boldsymbol{q}} W(\boldsymbol{p},\boldsymbol{q};\boldsymbol{k})\delta(\omega^{+}_{\boldsymbol{k}} - \omega^{+}_{\boldsymbol{p}} - \omega^{+}_{\boldsymbol{q}} - \omega^{-}_{\boldsymbol{k}-\boldsymbol{p}-\boldsymbol{q}}).\end{aligned} \tag{13}$$

Spontaneous magnon decay is kinematically allowed if the equation for the scattering surface,

$$\omega^{+}_{\boldsymbol{k}} = \omega^{+}_{\boldsymbol{p}} + \omega^{+}_{\boldsymbol{q}} + \omega^{-}_{\boldsymbol{k}-\boldsymbol{p}-\boldsymbol{q}}, \tag{14}$$

has nontrivial solutions. A similar problem of finding the scattering surface for the zero-temperature decay of quasiparticles with linear dispersion plus cubic nonlinearity has recently been discussed by O'Brien and Sushkov [15]. A crucial observation is that for small nonlinearity, the loop momenta $\boldsymbol{p}$ and $\boldsymbol{q}$ are almost aligned with the direction of the external momentum $\boldsymbol{k}$ as shown in Fig. 4(a). It is then convenient to project $\boldsymbol{p} = p_\parallel\hat{\boldsymbol{k}} + p_\perp\hat{\boldsymbol{k}}_\perp$ and $\boldsymbol{q} = q_\parallel\hat{\boldsymbol{k}} + q_\perp\hat{\boldsymbol{k}}_\perp$ onto the direction $\hat{\boldsymbol{k}} = \boldsymbol{k}/|\boldsymbol{k}|$ of the external momentum, where $\hat{\boldsymbol{k}}_\perp$ is a unit vector perpendicular to $\boldsymbol{k}$. Assuming that all momenta are small compared with the inverse lattice spacing, we may approximate the magnon dispersions in Eq. (14) by the small-momentum expansion [Eq. (5)]. Anticipating that the transverse components $p_\perp$ and $q_\perp$ are parametrically smaller than the longitudinal components $p_\parallel$, $q_\parallel$, and $k - p_\parallel - q_\parallel$, we may further expand up to quadratic order in $p_\perp$ and $q_\perp$. For $k \lesssim \min\{1/a, |mc|\}$, Eq. (14) for the scattering surface then reduces to

$$\frac{p_\perp^2}{p_\parallel} + \frac{q_\perp^2}{q_\parallel} + \frac{(p_\perp + q_\perp)^2}{k - p_\parallel - q_\parallel} = \frac{4\hat{k}_x\hat{k}_y}{mc}(k - p_\parallel)(k - q_\parallel). \tag{15}$$

Keeping in mind that momentum conservation requires $0 < p_\parallel < k$, $0 < q_\parallel < k$, and $0 < k - p_\parallel - q_\parallel < k$, the quadratic form on the left-hand side of Eq. (15) is positive definite. For $m > 0$, this implies that Eq. (15) has only a solution if $\hat{k}_x\hat{k}_y > 0$; i.e., $\boldsymbol{k}$ must lie in the first or in the third quadrant of the Brillouin zone. For fixed $p_\parallel$ and $q_\parallel$, the solution of Eq. (15) is then an ellipse in the $p_\perp$–$q_\perp$ plane, as illustrated in Fig. 4(b). The elliptic approximation to the scattering surface is accurate to leading order in ka and $k/|mc|$. For larger wave vectors, the shape of the scattering surfaces deviates from an ellipse, as illustrated in Fig. 4(c).

Let us now calculate the leading momentum dependence of the decay rate for $k \to 0$. In this long-wavelength limit, we

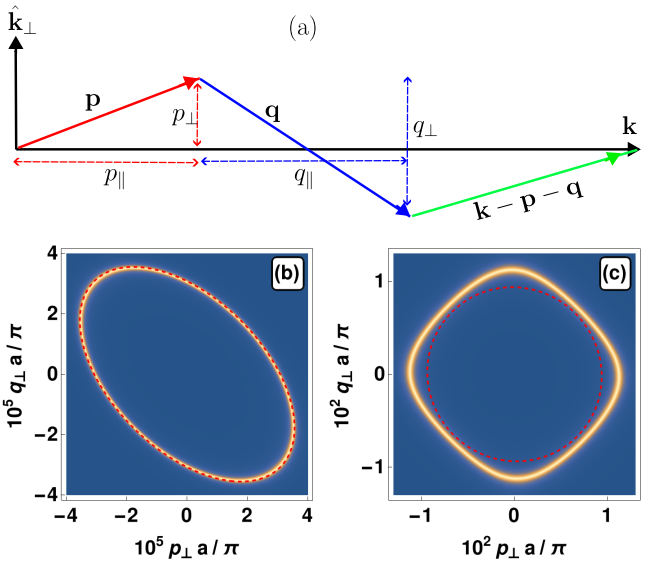


FIG. 4. (a) For small nonlinearity, energy and momentum conservation implies that the decay of one magnon with momentum $\boldsymbol{k}$ into three magnons with momenta $\boldsymbol{p}$, $\boldsymbol{q}$, and $\boldsymbol{k}-\boldsymbol{p}-\boldsymbol{q}$ is only possible if $\boldsymbol{p}$ and $\boldsymbol{q}$ are almost aligned with $\boldsymbol{k}$. (b) Elliptic scattering surface in the $p_\perp - q_\perp$ plane associated with spontaneous magnon decay. The red dashed line represents the solution of Eq. (15), which is valid for small ka and to leading order in $p_\perp/k$ and $q_\perp/k$. The yellow curve is obtained from the numerical solution of the original Eq. (14). We have chosen the following parameters: $D/J=-1/2$, $E/J=-1/4$, $k_x a = k_y a = 0.003\pi/\sqrt{2}$, and $p_\parallel a = q_\parallel a = 0.001\pi$. (c) For larger wave vectors, the shape of the scattering surface deviates from an ellipse.

may approximate the vertex in Eq. (12) by

$$\Gamma_0^{(2A)}(\mathbf{3};\mathbf{4};\mathbf{2},\mathbf{1}) = J\left[\sqrt{\frac{k_3k_4}{k_2k_1}}(1+\hat{\boldsymbol{k}}_3\cdot\hat{\boldsymbol{k}}_4)-\sqrt{\frac{k_2k_1}{k_3k_4}}(1-\hat{\boldsymbol{k}}_2\cdot\hat{\boldsymbol{k}}_1)\right]. \quad (16)$$

Note that in this limit the vertex is independent of the altermagnetic couplings D and E, so that magnon decay in altermagnets is due to the specific kinematics of the band splitting. Keeping in mind that for the scattering geometry of interest, the loop momenta $\boldsymbol{p}$ and $\boldsymbol{q}$ are almost parallel to the external momentum $\boldsymbol{k}$, the relevant squared matrix element can be approximated by

$$W(\boldsymbol{p},\boldsymbol{q};\boldsymbol{k}) = \frac{J^2}{4}\left[\sqrt{\frac{p_\parallel q_\parallel}{k(k-p_\parallel-q_\parallel)}}\left(\frac{p_\perp}{p_\parallel}-\frac{q_\perp}{q_\parallel}\right)^2 - \sqrt{\frac{k(k-p_\parallel-q_\parallel)}{p_\parallel q_\parallel}}\frac{(p_\perp+q_\perp)^2}{(k-p_\parallel-q_\parallel)^2}\right]^2. \quad (17)$$

Substituting this into Eq. (13) and using the elliptic approximation [Eq. (15)] for the scattering surface, we may scale out the momentum dependence by setting $p_\parallel = kx_1$, $q_\parallel = kx_2$ and $p_\perp = \sqrt{2k^3/|mc|}y_1$, $q_\perp = \sqrt{2k^3/|mc|}y_2$. Note that the transverse momenta scale as $k^{3/2}$, whereas the longitudinal momenta are of order k, so that for sufficiently small k our assumption that $p_\perp$ and $q_\perp$ are small compared with $p_\parallel$ and $q_\parallel$ is justified. The transverse integration over y_1 and y_2 can then be carried out analytically, while the remaining two-dimensional integral over x_1 and x_2 can be evaluated numerically. Our final result for the decay rate of α magnons is [16]

$$\gamma_\alpha(\boldsymbol{k}) = 0.0135\,\Theta\left(\frac{k_xk_y}{m}\right)\frac{J^2a^4|\boldsymbol{k}|k_x^2k_y^2}{m^2c^3}+\mathcal{O}(k^6), \quad (18)$$

where $\Theta(x)=1$ for $x>0$ and $\Theta(x)=0$ for $x<0$. The decay rate of the β magnons with chirality $p=-$ can be obtained by substituting $\Theta(k_xk_y/m)\to\Theta(-k_xk_y/m)$ in Eq. (18).

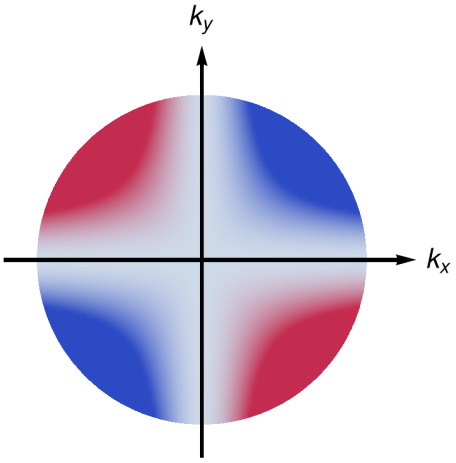


FIG. 5. Illustration of the chirality selectivity of the spontaneous magnon decay rate in two-dimensional altermagnets for small momenta. The intensity of the blue shading is proportional to the spontaneous decay rate $\gamma_\alpha(\boldsymbol{k})$ of the α magnon given in Eq. (18), while the red shading represents the corresponding decay rate $\gamma_\beta(\boldsymbol{k})$ of the β magnon. We only show the long-wavelength regime $|\boldsymbol{k}| \ll 1/a$, where the approximations leading to Eq. (18) are expected to be accurate.

IV. CONCLUSIONS

We conclude that spontaneous magnon decay in two-dimensional altermagnets is chirality selective: For positive m, the α magnons can spontaneously decay only in the first and third quadrants of the Brillouin zone, while the β magnons can decay only in the second and fourth quadrants. Moreover, the decay rates are maximal for momenta parallel to the diagonals of the Brillouin zone and vanish along the symmetry axes of the crystal, as illustrated in Fig. 5. Our result [Eq. (18)] should be compared with the Beliaev damping of sound in the ground state of the superfluid Bose gas, which is proportional k^3 in two dimensions [3]. In Eq. (18), two extra powers of k are generated by the strong momentum dependence of the squared scattering vertex in Eq. (17). This is similar to the XXZ ferromagnet [17], where the hydrodynamic momentum dependence of the scattering vertex generates four extra powers of k, so that the damping behaves as k^7 at long wavelengths. Note also that our result [Eq. (18)] for the damping at long wavelengths is not specific to the checkerboard model [Eq. (1)], but generic to all models with the same symmetries, since we expressed it in terms of the long-wavelength parameters c and m.

Because the calculations presented in this work are based on the bosonization of the spin operators using the Holstein-Primakoff transformation [13] and the expansion of the resulting boson Hamiltonian in powers of $1/S$, our results can only be expected to be quantitatively accurate for large spin S. An alternative bosonization of spin operators proposed by Dyson [18] and Maleev [19] avoids the formal expansion of the Hamiltonian in powers of $1/S$, at the price of mapping the spin Hamiltonian onto a non-Hermitian boson Hamiltonian. Although the Dyson-Maleev transformation has been successfully used to calculate magnon damping in quantum antiferromagnets [4,14], it completely fails in the present context because the non-Hermiticity of the Dyson-Maleev Hamiltonian leads to negative values of the product of scattering vertices in the diagrams shown in Fig. 3(b), implying unphysical negative decay rates. We are not aware of any other example for such a spectacular failure of the Dyson-Maleev transformation.

The anisotropy and chirality selectivity of spontaneous magnon decay in altermagnets offer possibilities of identifying altermagnets experimentally. For example, since magnons propagating along the symmetry axes of the crystal cannot spontaneously decay, while magnons propagating along the diagonals have the maximal possible decay rate, the transport of magnetization or heat along the symmetry axes is expected to be most efficient. A popular method for modeling transport phenomena in magnets is based on the Landau-Lifshitz-Gilbert equation [20], where the magnon damping is taken into account via a phenomenological damping rate. Our result that spontaneous magnon decay in two-dimensional altermagnets is anisotropic and chirality selective cannot be straightforwardly incorporated into the Gilbert damping phenomenology.

Note added. After completion of this work, we have become aware of independent complementary work on magnon decays. For details, see Ref. [9].

ACKNOWLEDGMENT

We thank the Deutsche Forschungsgemeinschaft (DFG, German Research Foundation) for financial support via TRR 288-422213477.

DATA AVAILABILITY

No data were created or analyzed in this study.

[1] E. M. Lifshitz and L. P. Pitaevskii, *Statistical Physics, Part 2* (Pergamon Press, Oxford, 1980).

[2] S. T. Beliaev, Energy-spectrum of a nonideal Bose gas, Zh. Eksp. Teor. Fiz. **34**, 433 (1958) [Sov. Phys. JETP **34**, 299 (1958)].

[3] A. Sinner, N. Hasselmann, and P. Kopietz, Spectral function and quasiparticle damping of interacting Bosons in two dimensions, Phys. Rev. Lett. **102**, 120601 (2009).

[4] A. B. Harris, D. Kumar, B. I. Halperin, and P. C. Hohenberg, Dynamics of an antiferromagnet at low temperatures: Spin-wave damping and hydrodynamics, Phys. Rev. B **3**, 961 (1971).

[5] M. E. Zhitomirsky and A. L. Chernyshev, *Colloquium:* Spontaneous magnon decays, Rev. Mod. Phys. **85**, 219 (2013).

[6] L. Šmejkal, J. Sinova, and T. Jungwirth, Beyond conventional ferromagnetism and antiferromagnetism: A phase with nonrelativistic spin and crystal rotation symmetry, Phys. Rev. X **12**, 031042 (2022).

[7] L. Šmejkal, J. Sinova, and T. Jungwirth, Emerging research landscape of altermagnetism, Phys. Rev. X **12**, 040501 (2022).

[8] L. Šmejkal, M. Marmodoro, K.-H. Ahn, R. Gonzalez-Hernandez, I. Turek, S. Mankowsky, H. Ebert, S. W. D'Souza, O. Sipr, J. Sinova, and T. Jungwirth, Chiral magnons in altermagnetic RuO_2, Phys. Rev. Lett. **131**, 256703 (2023).

[9] After completion of this work, we have become aware of independent complementary work on magnon decays in general models for two-dimensional altermagnets by Eto *et al.* [21], who agree with our results and also present numerical results for arbitrary momenta.

[10] F. Garcia-Gaitan, A. Kefayati, J. Q. Xiao, and B. K. Nikolic, Magnon spectrum of altermagnets: Time-dependent matrix product states vs. linearized Holstein-Primakoff calculations unravelling spontaneous magnon decay, Phys. Rev. B **111**, L020407 (2025).

[11] B. Brekke, A. Brataas, and A. Sudbo, Two-dimensional altermagnets: A minimal model, Phys. Rev. B **108**, 224421 (2023).

[12] P. M. Cônsoli and M. Vojta, SU(N) altermagnetism: Lattice models, magnon modes, and flavor-split bands, Phys. Rev. Lett. **134**, 196701 (2025).

[13] T. Holstein and H. Primakoff, Field dependence of the intrinsic domain magnetization of a ferromagnet, Phys. Rev. **58**, 1098 (1940).

[14] P. Kopietz, Magnon damping in the two-dimensional quantum Heisenberg antiferromagnet at short wavelengths, Phys. Rev. B **41**, 9228 (1990).

[15] M. C. O'Brien and O. P. Sushkov, Colossal quasiparticle radiation in the Lifshitz spin liquid phase of a two-dimensional quantum antiferromagnet, Phys. Rev. B **101**, 184408 (2020).

[16] Corrections from the real part of the magnon self-energy can be implicitly taken into account by redefining the long-wavelength parameters c and $1/m$ that characterize the magnon dispersion [Eq. (5)].

[17] V. A. Stephanovich and M. E. Zhitomirsky, Spontaneous magnon decays in planar ferromagnet, Europhys. Lett. **95**, 17007 (2011).

[18] F. D. Dyson, General theory of spin-wave interactions, Phys. Rev. **102**, 1217 (1956).

[19] S. V. Maleev, Scattering of slow neutrons in ferromagnets, Zh. Eksp. Teor. Fiz. **33**, 1010 (1957) [Sov. Phys. JETP **33**, 776 (1958)].

[20] A. G. Gurevich and G. A. Melkov, *Magnetization Oscillations and Waves* (CRC Press, Boca Raton, FL, 1996).

[21] R. Eto, M. Gohlke, J. Sinova, M. Mochizuki, A. L. Chernyshev, and A. Mook, Spontaneous magnon decays from nonrelativistic time-reversal symmetry breaking in altermagnets, arXiv:2502.20146v1.